2019

Noninvasive quantification of axonal loss in the presence of tissue swelling in traumatic spinal cord injury mice

Tsen-Hsuan Lin
Washington University School of Medicine in St. Louis

Peng Sun
Washington University School of Medicine in St. Louis

Mitchell Hallman
Washington University School of Medicine in St. Louis

Fay C. Hwang
Washington University School of Medicine in St. Louis

Michael Wallendorf
Washington University School of Medicine in St. Louis

See next page for additional authors

JOURNAL OF NEUROTRAUMA 36:2308–2315 (August 1, 2019)

DOI: 10.1089/neu.2018.6016

Noninvasive Quantification of Axonal Loss in the Presence of Tissue Swelling in Traumatic Spinal Cord Injury Mice

Tsen-Hsuan Lin,[1,**] Peng Sun,[1,**] Mitchell Hallman,[1,*] Fay C. Hwang,[1] Michael Wallendorf,[2] Wilson Z. Ray,[3–5] William M. Spees,[1,3] and Sheng-Kwei Song[1,3,5]

Abstract

Neuroimaging plays an important role in assessing axonal pathology after traumatic spinal cord injury. However, co-existing inflammation confounds imaging assessment of the severity of axonal injury. Herein, we applied diffusion basis spectrum imaging (DBSI) to quantitatively differentiate and quantify underlying pathologies in traumatic spinal cord injury at 3 days post-injury. Results reveal that DBSI was capable of detecting and differentiating axonal injury, demyelination, and inflammation-associated edema and cell infiltration in contusion-injured spinal cords. DBSI was able to detect and quantify axonal loss in the presence of white matter tract swelling. The DBSI-defined apparent axonal volume correlated with the corresponding histological markers. DBSI-derived pathological metrics could serve as neuroimaging biomarkers to differentiate and quantify coexisting white matter pathologies in spinal cord injury, providing potential surrogate outcome measures to assess spinal cord injury progression and response to therapies.

Keywords: axonal injury; axonal volume; demyelination; diffusion MRI; inflammation; lesion cavity; spinal cord injury

Introduction

Traumatic spinal cord injury (SCI) is devastating. Acute medical and surgical interventions have been beneficial to reduce secondary damage and promote axonal preservation.[1,2] However, recovery of neurological impairments remains an unmet challenge in SCI. Traumatic contusion leads to coexisting axonal injury/loss, demyelination, and inflammation in the injured spinal cord. Among these pathologies, axonal loss likely plays a crucial role in long-term neurological impairments.[3–5] Early therapeutic interventions to preserve axonal integrity may potentially prevent injury progression. Therefore, developing a suitable assessment of axonal loss at all phases of SCI could significantly impact prognosis and treatment stratification.

Several neuroimaging methods have been used to elucidate structural integrity after SCI.[6] Diffusion tensor imaging (DTI) has been applied to noninvasively detect structural changes and axonal damage in the central nervous system that occur in SCI.[7] In earlier work, decreased DTI-derived axial diffusivity ($\lambda_{\parallel}$) and increased radial diffusivity ($\lambda_{\perp}$) have been shown to reflect axonal injury and demyelination in animal models, respectively.[8–13] However, accumulated evidence suggested that inflammation (a hallmark of SCI)[14] and axonal loss (highly associated with irreversible neurological disability)[3] can confound the DTI assessment of axon or myelin injury.[12,15,16] To eliminate these confounds, we developed diffusion basis spectrum imaging (DBSI) to separate contributions of the multiple coexisting pathologies that often exist in various white matter diseases.[17] For instance, DBSI has been applied in studies of optic nerve, corpus callosum and spinal cord in multiple sclerosis patients and animal models, where it successfully identified coexisting inflammatory cell infiltration and vasogenic edema, axonal injury and demyelination.[12,17–19] In cervical spondylotic myelopathy (CSM) patients, we successfully applied DBSI to detect axonal loss in cervical spinal cord.[20] The DBSI-detected axonal loss correlated well with clinical functional assessments, suggesting DBSI could potentially serve as an outcome measure to predict neurological impairment in CSM.[20]

In the present study, we applied DBSI to assess spinal cord pathologies in SCI mice 3 days after contusion injury. DBSI detected axonal injury, demyelination, inflammatory cell infiltration, and vasogenic edema in spinal cord white matter in these mice. We observed an acute $\sim$13% axonal loss in spinal cord white matter tracts in SCI mice despite severe tissue swelling. The DBSI results were supported by corresponding histological markers.

Methods

Spinal cord injury

All experimental procedures were approved by the Washington University Institutional Animal Care and Use Committee and performed according to the Public Health Service Policy on

[1]Department of Radiology, [2]Department of Biostatistics, [3]Hope Center for Neurological Disorders, [4]Department of Neurosurgery, [5]Department of Biomedical Engineering, Washington University, St. Louis, Missouri.
*Current affiliation: Perelman School of Medicine at the University of Pennsylvania, Philadelphia, Pennsylvania.
**These authors contributed equally to this work.

Humane Care and Use of Laboratory Animals *Guide for the Care and Use of Laboratory Animals* (Institute of Laboratory Animal Resource, National Research Council, 1996). Sixteen 10-week-old female C57BL/6 mice (Jackson Laboratory, Bar Harbor, ME) weighing ~20 g were housed in the Washington University animal facility with a 12-h light/dark cycle. Before surgery, mice were anesthetized via intraperitoneal injection of a mixture of ketamine (80 mg/kg) and xylazine (10 mg/kg). A spinal cord impactor device, modified from the device developed at Ohio State University, was employed to produce spinal cord contusion injury.[21] Modifications included a flexure-based design in which the extent of overshoot was reduced with a micrometer-control and mechanical stop.[22] For contusion injury, a 1.3-mm-diameter round tip and 0.1 m/sec impact speed were used.

The skin above the vertebral column of all mice was shaved and cleaned with betadine. A 15-mm midline skin incision was made and the vertebral column was exposed. After the spinal thoracic region was exposed by separation of dorsal muscles to the side, the spinous processes of T8–T13 vertebrae were exposed. A laminectomy was performed at vertebral level T10 and half of T9 to expose the dorsal cord surface with dura remaining intact. The vertebral column was stabilized with angled clamps on the T8 and T12 transverse processes and then SCI was induced using the spinal cord impactor. After laminectomy, 10 mice received 0.8-mm displacement contusion at the T9 vertebral level. The other six mice received no contusion to serve as the sham control. After surgery, the wound was closed in layers with 5-0 polyglactin and nylon sutures. Enrofloxacin (2.5 mg/kg) and lactated Ringer's solution (1 mL) were injected subcutaneously.

Diffusion magnetic resonance imaging

In vivo diffusion magnetic resonance imaging (MRI) measurements were performed 3 days after SCI or laminectomy on a 4.7 T Agilent DirectDrive™ small-animal MRI system (Agilent Technologies, Santa Clara, CA) equipped with a Magnex/Agilent HD imaging gradient coil (Magnex/Agilent, Oxford, UK), capable of pulse gradient strengths up to 58 G/cm (=580 mT/m) and a gradient rise time ≤295 μsec. Mice were anesthetized with ~1.0–1.5% isoflurane in oxygen during scans. Breathing rate was monitored and body temperature was maintained at 37°C with a small animal physiological monitoring and control unit (SA Instruments, Stony Brook, NY). The respiratory exhaust line was connected to a pressure transducer to synchronize diffusion-weighted MRI acquisition with the animal's respiratory rate. An actively decoupled volume (transmit)/surface (receive) coil pair, covering the T8 – T11 vertebral segments (15 mm × 8 mm), was used for MRI excitation and signal reception.[23]

Diffusion-weighted MRI data were acquired using a conventional spin-echo diffusion-weighted sequence with an icosahedral 25-direction diffusion-encoding scheme[24] with one b=0 image. Diffusion-weighted magnetic resonance acquisition parameters were repetition time (TR) of ~0.3 sec (TR was slightly varied due to respiratory gating), echo time of 43 msec, time between gradient pulses (Δ) of 25 msec, gradient pulse duration (δ) of 6 msec, maximum b-value of 2200 sec/mm^2 (each of the diffusion encodings have a unique b-value and direction), slice thickness of 1.8 mm, field-of-view of 10 × 10 mm^2, and data matrix of 96 × 96 (i.e., in-plane resolution of 104 × 104 μm^2).

Diffusion-weighted MRI data analysis

Data was analyzed with both DBSI and conventional DTI analysis packages developed in-house and running in Matlab.[17,25] For spinal cord white matter tracts (coherent fiber bundles), the diffusion-weighted imaging data was modeled according to Equation [1]:

$$S_k = f_{fiber} e^{-|\vec{b_k}|\lambda_\perp} e^{-|\vec{b_k}|(\lambda_{||}-\lambda_\perp)\cos^2\Phi_k} + \int_a^b f(D) e^{-|\vec{b_k}|D} dD \quad (k = 1,\ 2,\ 3,\ \ldots,\ 25). \qquad [1]$$

The quantities S_k and $\left|\overrightarrow{b_k}\right|$ are the signal and b-value of the k^{th} diffusion gradient, Φ_k is the angle between the k^{th} diffusion gradient and the principal direction of the anisotropic tensor, $\lambda_{||}$ and $\lambda_\perp$ are the axial and radial diffusivities of the anisotropic tensor, f_{fiber} is the signal intensity fraction for the anisotropic tensor, and a and b are the low and high diffusivity limits for the isotropic diffusion spectrum $f(D)$. DBSI-derived f_{fiber} represents spinal cord white matter tract density in an image voxel. DBSI-derived $\lambda_{||}$ and $\lambda_\perp$ reflect residual axon and myelin integrity respectively: $\downarrow \lambda_{||} \approx$ axonal injury and $\uparrow \lambda_\perp \approx$ demyelination.[12,17,25,26] Based on our previous experimental findings, the restricted isotropic diffusion fraction reflecting cellularity is derived by the summation of $f(D)$ at $0 \le$ ADC $\le 0.3\ \mu$m^2/msec. The summation of the remaining $f(D)$ at $0.3 <$ ADC $\le 3\ \mu$m^2/msec represents non-restricted isotropic diffusion, which putatively denotes vasogenic edema and cerebrospinal fluid.[12,17,25,26]

Regions of interest (ROIs) were manually drawn in ventral and lateral white matter tracts on the diffusion-weighted image, corresponding to the diffusion gradient direction perpendicular to white matter fiber tracts (with good gray-white matter contrast), to minimize partial volume effects. ROIs were then transferred to the parametric maps to calculate each of the DBSI- and DTI-derived pathological metrics (e.g., Fig. 1A).

DBSI-derived axonal volume

To assess the extent of axonal loss, DBSI-derived axonal volume was computed by multiplying DBSI fiber fraction, f_{fiber} (the density of fiber tract within a given image voxel, which may also be affected by infiltrating cells, vasogenic edema, and gray matter) by the corresponding volume of the ROI. Note that in the case of tissue swelling after SCI, the number of voxels occupied by the white matter tracts would increase with peripheral/distant voxels only partially occupied by the swollen tracts (reflected by reduced fiber density). Thus, multiplication of f_{fiber} and voxel volume will derive an ''apparent'' axonal volume (with a unit of mL or μL), linearly correlating with axon counts although not a real axonal volume.

Immunohistochemistry

Immediately after the *in vivo* diffusion MRI data acquisition, mice were deeply anesthetized and underwent perfusion-fixation via the left cardiac ventricle with phosphate-buffered saline (PBS) followed by 4% paraformaldehyde (PFA). Spines were excised and stored in 4% PFA at 4°C for 24 h, then transferred to PBS for further storage until processing. The 2-mm segment of spinal cord centered at the contusion epicenter was dissected, decalcified with the vertebral column intact, and embedded in paraffin wax. Paraffin blocks were sectioned at 5-μm thick, deparaffinized, and rehydrated for immunohistochemistry (IHC) analysis. Sections were blocked with 5% normal goat serum and 1% bovine serum albumin in PBS for 30 min at room temperature to prevent non-specific binding. Slides were then incubated overnight at 4°C with primary antibody and then 1 h at room temperature with the appropriate secondary antibody. Primary antibodies used were anti-total neurofilament (SMI-312, BioLegend, 1:300), anti-phosphorylated neurofilament (SMI-31, BioLegend, 1:300), and anti-myelin basic protein (MBP; Sigma, 1:300). Secondary antibodies were goat anti-mouse or goat anti-rabbit (Invitrogen, 1:240) conjugated to either Alexa 488 for SMI-31/SMI-312 or Alexa 594 for MBP.

Slides were mounted with Vectashield Mounting Medium for 4′,6-diamidino-2-phenylindole (DAPI; Vector Laboratory, Inc.,

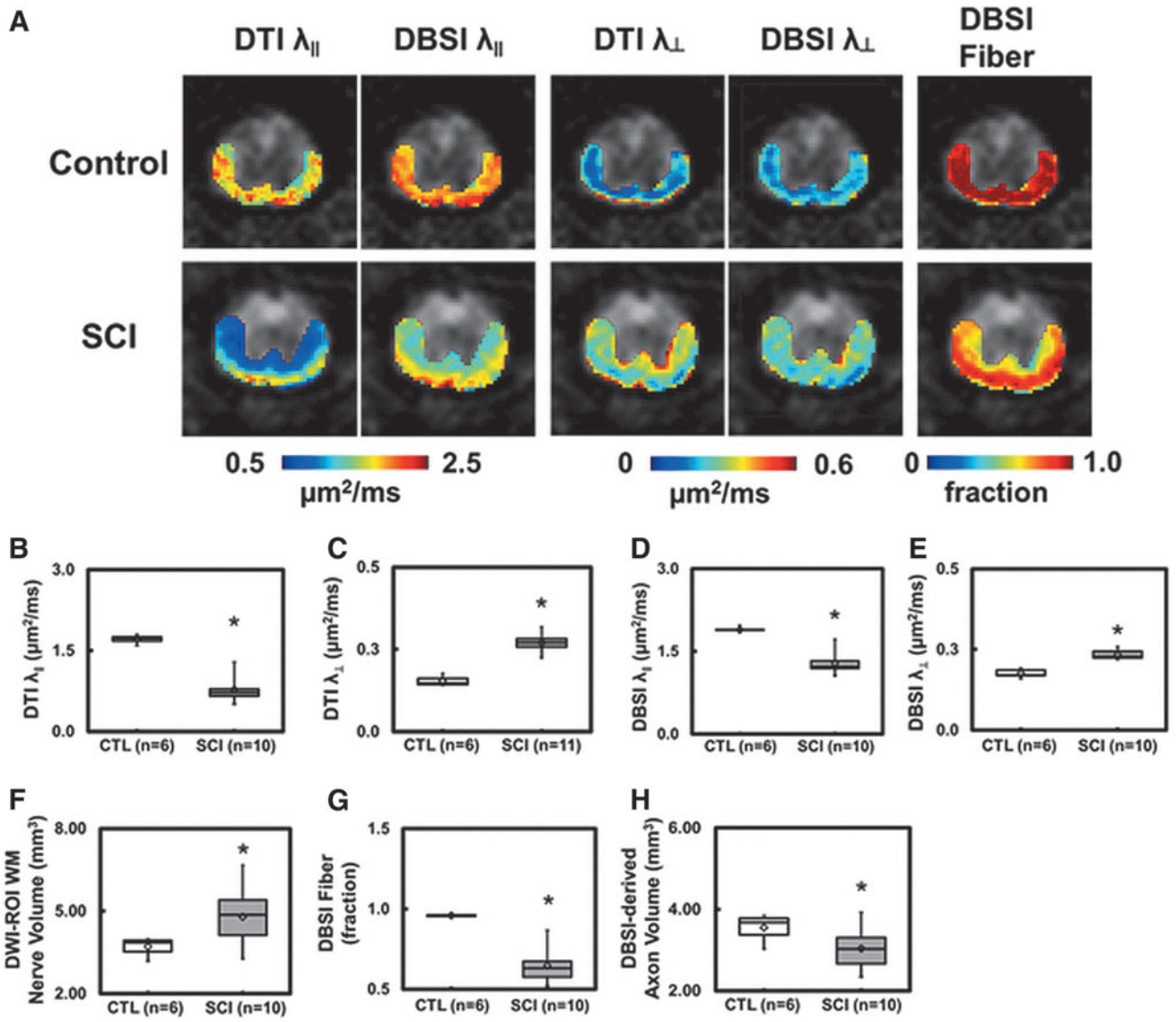

FIG. 1. Representative *in vivo* diffusion tensor imaging (DTI) and diffusion basis spectrum imaging (DBSI) metric maps were overlaid on gray-scale diffusion-weighted images from one control and one spinal cord injury (SCI) mouse at T9 vertebral level **(A).** DTI axon/myelin pathological metrics are susceptible to the effect of co-existing inflammation and axonal loss that could exaggerate or underestimate the severity of SCI. In the present study, inflammatory cell infiltration resulted in a more significantly decreased DTI axial diffusivity ($\lambda_{\|}$) **(B)** than that derived by DBSI **(D),** while the combined axonal loss and vasogenic edema led to a more significantly increased DTI radial diffusivity ($\lambda_{\perp}$) **(C)** than DBSI $\lambda_{\perp}$ **(E).** Increased white matter volume (**F**; as a result of cell infiltration and vasogenic edema) and decreased DBSI fiber fraction (**G**; the decreased axonal density as a result of combined effects of increased cell infiltration, vasogenic edema, and axonal loss) were present at 3 days after SCI. DBSI-derived axonal volume **(H)** derived as the product of white matter volume (F) times DBSI fiber fraction (G) reflects the extent of axonal loss in the presence of tissue swelling. At this time-point, decreased DBSI-derived apparent axonal volume was observed, suggesting axonal loss (H). The intensity gradients in DBSI $\lambda_{\|}$, $\lambda_{\perp}$, and fiber fraction maps reflect spatial variation of injury severity that are intrinsic to the dorsal-to-ventral impact nature of this SCI model. $^{*}p < 0.05$.

Burlingame, CA) and cover-slipped. Images were acquired on a Nikon Eclipse 80i fluorescence microscope with MetaMorph software (Universal Imaging Corporation, Sunnyvale, CA) at 10× and 20× magnifications. Quantification was performed on the entire 10× IHC ventral and lateral white matter tract images using ImageJ. Images then underwent background subtraction, bilateral filtering for edge preservation, watershed segmentation, and threshold determination. The analyze-particles-macro was then performed on SMI-312 and SMI-31 to count numbers of total and intact axons. The MBP area calculation was then normalized to the entire area of white matter column.[27,28] Background subtraction, threshold determination, and analyze particles were also used for counting DAPI-positive staining (National Institutes of Health [NIH]; https://imagej.nih.gov/ij).

Hematoxylin and eosin staining

We stained 5-μm paraffin slices with hematoxylin and eosin (H&E). Histological slices were scanned with an Olympus Nanozoomer slide scanner (Hamamatsu Photonics, Hamamatsu, Japan). For quantification analysis, background subtraction, bilateral filter for edge preservation, threshold determination, and analyze particles were also used for counting cavity voids (https://imagej.nih.gov/ij).

Statistical analysis

For all the boxplots, whiskers extend to the minimum/maximum and the mean is marked as diamonds. A two-sample t-test was performed between control and SCI groups. The correlation of histology data and DTI or DBSI measurements was analyzed by simple linear regression using the SAS REG procedure. All results are presented as mean ± standard deviation.

Results

Axonal injury, demyelination, and axonal loss in SCI

Representative DTI- and DBSI-axial ($\lambda_{\parallel}$) and radial diffusivity ($\lambda_{\perp}$) maps from one control and one SCI mouse are shown to demonstrate the presence of axonal injury and demyelination in spinal cord white matter tracts 3 days after injury. A 55% and 32% decrease in DTI- and DBSI-$\lambda_{\parallel}$, and 75% and 30% increase in DTI- and DBSI-$\lambda_{\perp}$, respectively, was observed (Fig. 1A-E). Larger changes in DTI-$\lambda_{\parallel}$ (Fig. 1B) and $\lambda_{\perp}$ (Fig. 1C) are seen compared with those derived by DBSI. Lower DBSI-derived fiber fraction (0.96 ± 0.01 vs. 0.65 ± 0.10, control vs. SCI) and white matter tract swelling (assessed by anatomical white matter tract volume: 3.70 ± 0.33 vs. $4.73 \pm 1.00\,mm^3$, control vs. SCI) were observed in SCI mice (Fig. 1A, 1F, 1G). DBSI-derived apparent axonal volume decreased in SCI mice (3.44 ± 0.33 vs. $3.01 \pm 0.46\,mm^3$, control vs. SCI; Fig. 1H), revealing axonal loss at 3 days after contusion.

Acute inflammation in SCI

DBSI-derived restricted (0.02 ± 0.01 vs. 0.16 ± 0.04, control vs. SCI, $p < 0.0001$; Fig. 2B) and non-restricted (0.01 ± 0.01 vs. 0.18 ± 0.06, control vs. SCI, $p < 0.0001$; Fig. 2B) isotropic diffusion fractions increased in the epicenter 3 days after SCI.

IHC of spinal cords

Post-DBSI IHC staining of spinal cords showed significant spinal cord white matter tract swelling (Fig. 3B, 3C). SCI spinal cords exhibited reduced SMI-31 staining intensity (Fig. 3B, 3C), suggesting axonal injury. Triple staining of control spinal cord, with SMI-312 (green), MBP (red), and DAPI (blue) antibodies (Fig. 3D), revealed high axonal density and intact myelin sheath with positive yellow staining, that is, positive SMI-312 (green) + MBP (red), and low DAPI density (blue). Control spinal cords exhibited negligible axon/myelin injury or cell infiltration (Fig. 3a, 3d, and 3g). SCI spinal cords exhibited increased axonal caliber (Fig. 3b, 3c; white arrows), decreased axon and myelin intensity, and increased DAPI density, suggesting coexisting axonal swelling/injury/loss, demyelination, and increased cell infiltration (Fig. 3b, 3c, 3e, 3f, 3h, and 3i).

Correlating DBSI with histology

H&E staining of spinal cords was used to assess tissue loss. Increased numbers of tissue voids were observed in SCI spinal cords (Fig. 4B, 4C). The area of tissue voids was automatically

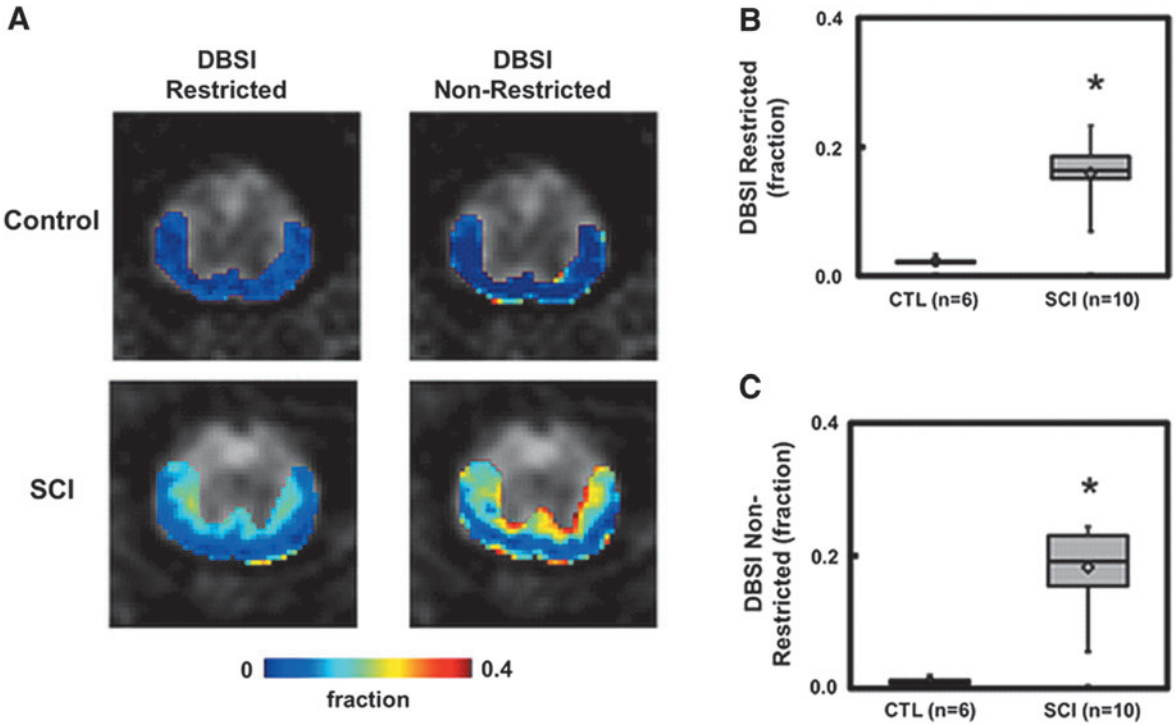

FIG. 2. One of the most unique features of diffusion basis spectrum imaging (DBSI) is its ability to quantify the changes associated with inflammation (i.e., the increased cellularity and vasogenic edema). Representative DBSI restricted and non-restricted isotropic diffusion fraction maps, are overlaid on grayscale diffusion-weighted images from one control and one spinal cord injury (SCI) mouse at T9 vertebral level to demonstrate the effectiveness of DBSI in detecting inflammation associated changes in SCI **(A).** Inflammatory cell infiltration and edema formation due to SCI is clearly reflected by the significantly increased restricted and non-restricted isotropic diffusion tensor fractions (**B** and **C**). The gradient in cellularity and edema, consistent with the similar gradient of axonal injury and demyelination assessed by anisotropic diffusion metrics in Figure 1, reflects the dorsal-ventral impact of this SCI model. *$p < 0.05$.

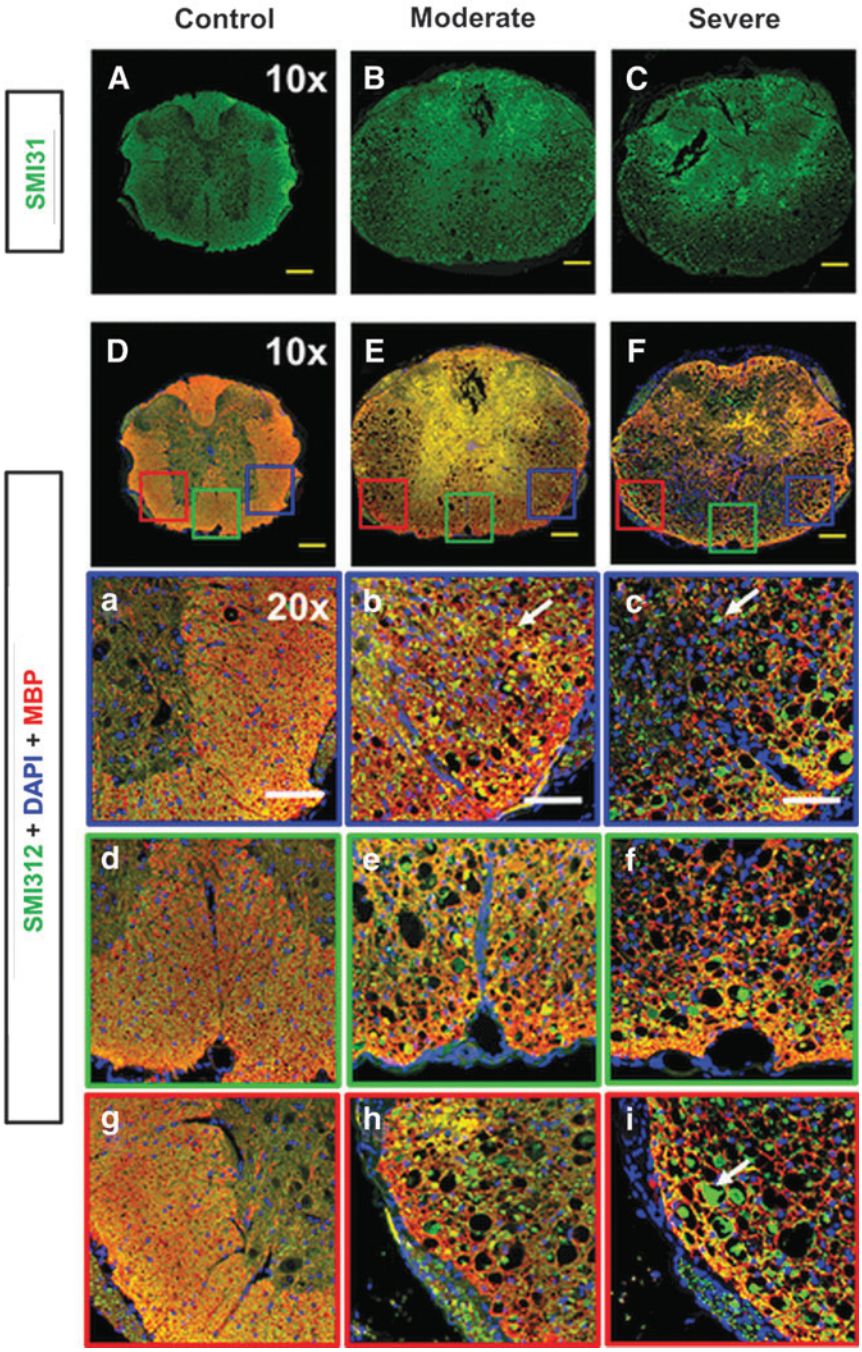

FIG. 3. Representative immunohistochemistry (IHC) SMI-31 (phosphorylated neurofilament, intact axons, green) and triple staining with SMI-312 (anti-total neurofilament, total axons, green), MBP (myelin basic protein, myelin sheaths, red), and DAPI (4′,6-dianidino-2-phenylindole, cell nuclei, blue) from one control and two spinal cord injury (SCI) with different injury severities (based on tissue damage). Compared with a control mouse **(A, D),** white matter swelling was obviously seen in SCI mice under 10× images (**B, C, E, F**). Reduced SMI-31 signal intensity in SCI mice (B, C) suggests axonal injury. Three representative 20× zoom-in triple IHC stained images of right **(a, b, c),** middle **(d, e, f),** and left **(g, h, i)** ventral white matter column from each spinal cord is presented. The control mouse (a, d, g) demonstrated dense yellow staining reflecting high density and strong signal intensity from SMI-312 (green) and MBP (red) with light DAPI (blue). The larger green spots (white arrows), reduced yellow-staining signal (combined with green and red), and increased voids in both moderate and severe spinal cords suggest co-existing axonal swelling, injury, demyelination and axonal loss (b, c, e, f, h, i). Increased DAPI staining (blue) is also seen in both SCI mice, associated with cell infiltration (b, c, e, f, h, i). Yellow scale bar in 10×: 200 μm. White scale bar in 20×: 100 μm.

segmented via multiple Gaussian function analysis (Fig. 4E; red curve). After thresholding was applied to the raw images (Fig. 4D), the area of tissue voids was segmented (Fig. 4F). The extracellular space (void) fraction was calculated by the ratio of masked area over the total area.

DBSI-derived $\lambda_{\parallel}$ and $\lambda_{\perp}$ correlated with SMI-31 counts (Fig. 5A; $r^2 = 0.76$, $p = 0.0004$) and MBP area fraction (Fig. 5B; $r^2 = 0.78$, $p = 0.0007$), respectively. DBSI-derived apparent ''axonal volume'' was consistent with SMI-312 area attenuation (Fig. 5C; $r^2 = 0.46$, $p = 0.0456$). DBSI restricted fraction correlated with

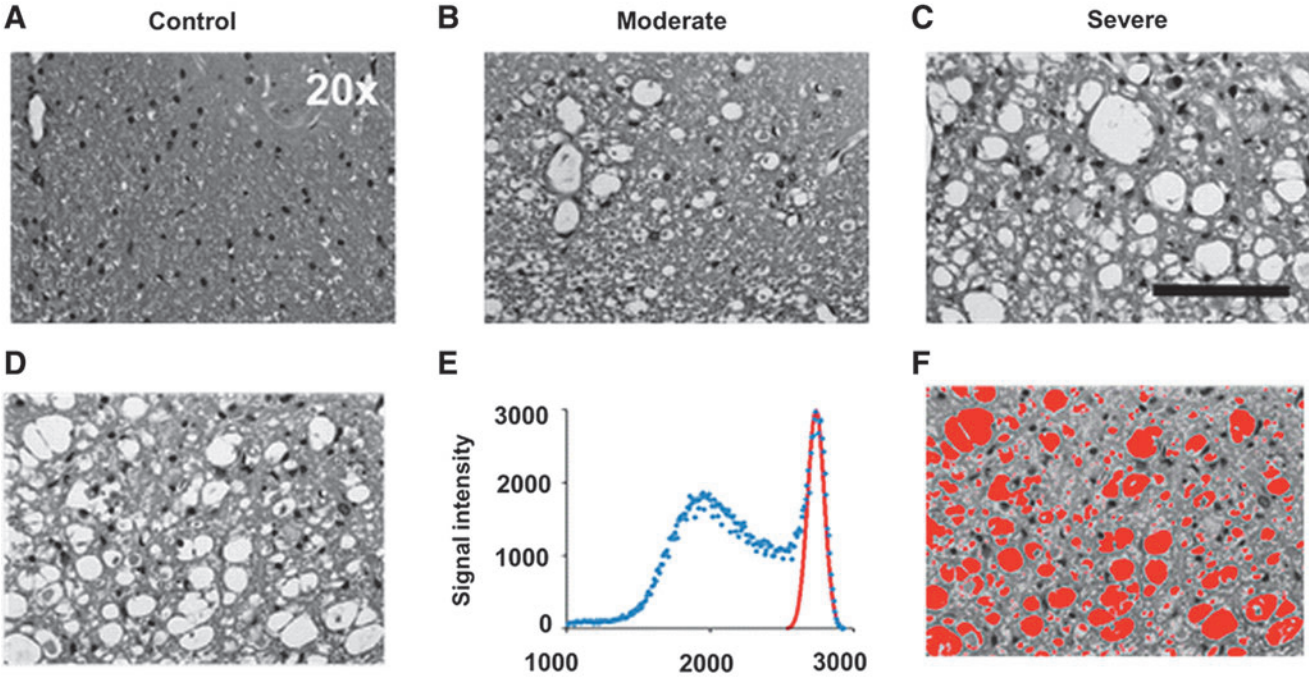

FIG. 4. Representative hematoxylin and eosin (H&E) images from one control **(A)** and two spinal cord injury **(B, C)** mice reveal the different degrees of tissue loss at 3 days after injury. The signal intensity histogram of the raw H&E image **(D)** is shown as blue dots of the signal-intensity histogram **(E).** After deconvolution of raw signal intensity using multiple Gaussian functions, the highest signal portion of the image was identified (E; red Gaussian curve). Applying this component to the raw H&E image in (D), the extracellular space (**F**; red area) was automatically identified and quantified. Black scale bar in 20×: 100 μm.

DAPI density (Fig. 5D; $r^2=0.63$, $p=0.0021$). The DBSI non-restricted (putatively edema plus free water; ADC >0.3 μm^2/msec) fraction correlated with tissue voids in H&E staining (Fig. 5E; $r^2=0.57$, $p=0.0028$). The data suggested that DBSI was able to quantitatively assess variable axonal injury (Fig. 5A), myelin damage (Fig. 5B), and inflammatory cell infiltration (Fig. 5D). Meanwhile, DBSI could also show the potential to reflect axonal loss (Fig. 5C). DTI-derived $\lambda_{\parallel}$ and $\lambda_{\perp}$ were consistent with SMI-31 counts (Fig. 5F; $r^2=0.85$, $p<0.0001$) and MBP area fraction (Fig. 5G; $r^2=0.71$, $p=0.0022$). However, increased cellularity and vasogenic edema were highly associated with exaggerated correlations in DTI results.

Discussion

In this study, we applied DBSI to assess mouse traumatic SCI 3 days after injury, avoiding the confounds of multiple coexisting pathologies on diffusion MRI metrics. Our results suggest that SCI mice developed axonal swelling, axonal injury, demyelination, and inflammation, as well as axonal loss at 72 h following contusion injury. The *in vivo* DBSI pathological metrics correlated with the corresponding postmortem histology markers, suggesting DBSI could potentially provide biomarkers to noninvasively reflect co-existing pathologies in SCI.

We previously introduced DTI $\lambda_{\parallel}$ and $\lambda_{\perp}$ to reflect axon and myelin integrity, respectively, in central nervous system (CNS) white matter tracts.[11,13,29,30] We subsequently reported DTI $\lambda_{\parallel}$ recovery after 1 day post-injury but did not return to the baseline values, and the DTI $\lambda_{\perp}$ gradually increased. Both DTI $\lambda_{\parallel}$ and $\lambda_{\perp}$ reached plateau from 7–14 days after injury.[11] Inflammation also plays a role in impeding axonal conduction,[31] thus functional recovery may directly or indirectly be related to the status of inflammation. The observed DTI $\lambda_{\parallel}$ and $\lambda_{\perp}$ profile did not purely reflect axonal injury and demyelination alone. It is likely also related to the evolution of inflammatory response and tissue loss.[12] Therefore, DTI $\lambda_{\parallel}$, $\lambda_{\perp}$, and fractional anisotropy do not appropriately reflect axonal recovery, even though it did show a correlation with functional recovery.[14,32] In the present study, we experimentally demonstrated the confounding effects of coexisting inflammation, e.g., overestimation of the axonal injury or myelin damage severity (Fig. 5 A-D). These confounding effects on conventional DTI are not resolved in other advanced diffusion techniques, such as Q-ball imaging,[33] diffusion kurtosis imaging,[34,35] composite hindered and restricted model of diffusion,[36,37] or neurite orientation dispersion and density imaging.[38,39] In the current study, with histological validation, we further confirmed that DBSI metrics can be used to successfully distinguish and quantify coexisting CNS pathologies 3 days after SCI in mice.[12,17–19,25]

At the observed time-point (72-h after spinal cord contusion), the injury site exhibited altered tissue perfusion, increased permeability of immune cells, and accumulated extracellular fluids.[19,29,30] White matter tract swelling (Fig. 1F and Fig. 3), due to cytotoxic/vasogenic edema and cell infiltration, confounds conventional diffusion MRI metrics. DBSI-derived non-restricted and restricted isotropic diffusion components accurately reflected the corresponding inflammatory pathology (i.e., vasogenic edema and inflammatory cell infiltration; Fig. 2). In addition, the lesion cavity is a prominent characteristic of contusion SCI, caused by central hemorrhagic necrosis.[14,40] These fluid-filled tissue voids will contribute to the DBSI non-restricted fraction (0.3 < ADC ≤3 μm^2/msec). Thus, at the 72-h time-point, the DBSI non-restricted fraction identifies the degree of lesion cavity formation in this SCI model (Fig. 5E).

Axonal damage and loss are recognized as important predictors for long-term irreversible neurological disability.[41–43] We have reported that the DBSI-derived apparent axonal volume (i.e., DBSI fiber fraction multiplied by corresponding ventrolateral white matter voxel

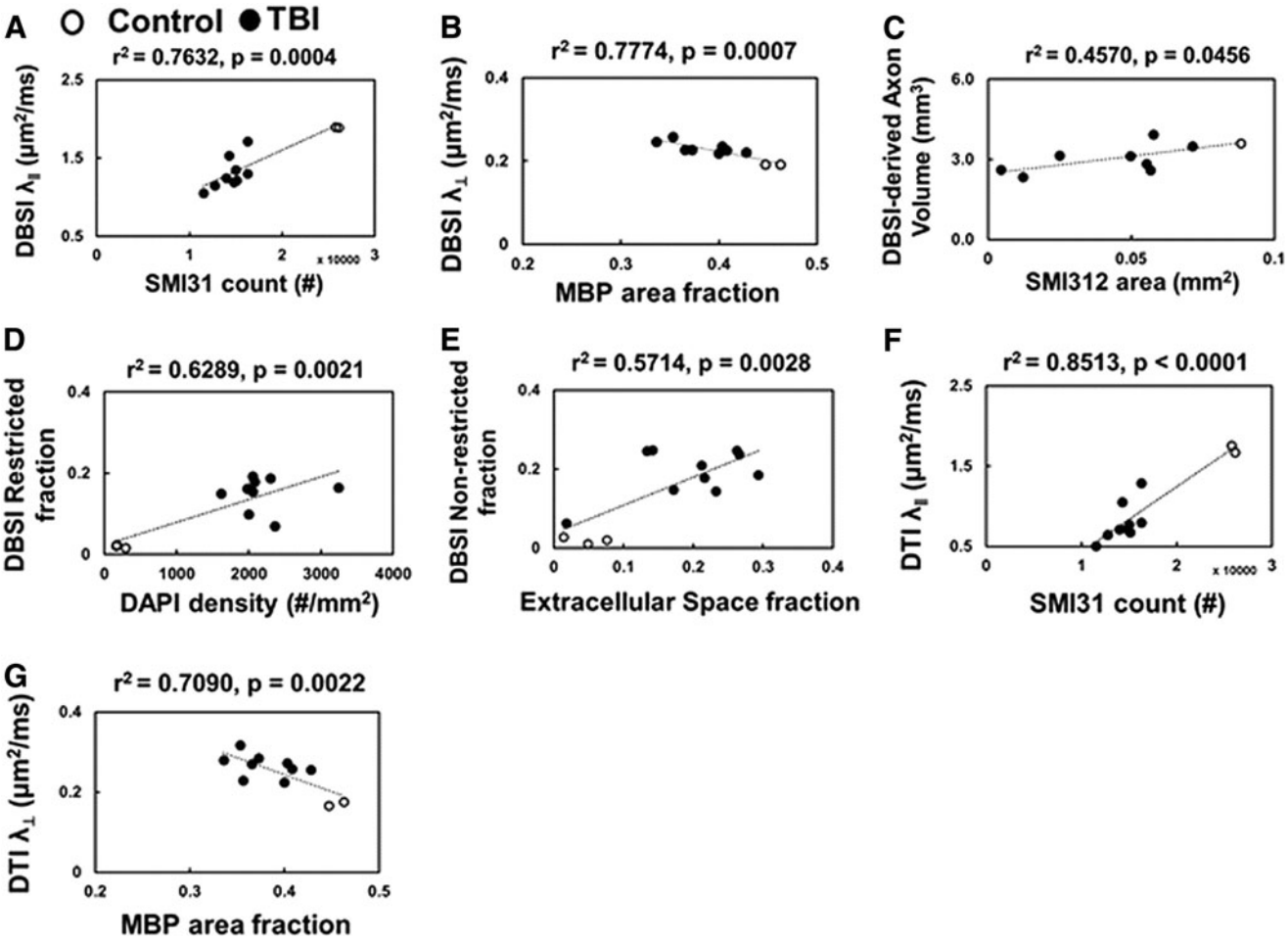

FIG. 5. Diffusion basis spectrum imaging (DBSI) axial diffusivity ($\lambda_{\parallel}$) and radial diffusivity ($\lambda_{\perp}$), and DBSI-derived axon volume correlated with SMI-31 counts **(A),** myelin basic protein (MBP) area **(B),** and SMI-312 area **(C),** respectively, suggesting DBSI accurately reflects axon/myelin damage, inflammatory cell infiltration. DBSI-restricted isotropic diffusion fraction (putative cellularity) correlates with 4′,6-dianidino-2-phenylindole (DAPI) density **(D)**. DBSI non-restricted (putatively edema and tissue loss) also correlated with different degree of extracellular space (voids) in hematoxylin and eosin **(E),** reflect the extent of lost tissues. Diffusion tensor imaging (DTI) ($\lambda_{\parallel}$ and $\lambda_{\perp}$ were consistent with SMI-31 counts **(F),** MBP area **(G),** but appear somewhat exaggerated compared with DBSI $\lambda_{\parallel}$ and $\lambda_{\perp}$ due to increased cellularity and vasogenic edema associated with inflammation (see Fig. 2).

volume) positively correlated with clinical behavioral function in CSM patients.[20] At the acute stage, the gradient of DBSI $\lambda_{\parallel}$ and $\lambda_{\perp}$ maps in SCI mouse reflected more severe injury at the inner ventrolateral white matter (Fig. 1A). The DBSI-derived anisotropic diffusion tensor components detected the effect of subsequent Wallerian degeneration resulting from excitotoxicity, damage of mitochondria, and energy depletion (Fig. 1).[14,44] The DBSI-derived axonal volume assessed axonal loss, ''seeing through'' white matter tract swelling arising from inflammation (Fig. 1G, 1H). These findings quantitatively addressed the insufficiency of conventional DTI models, which assume single tensor diffusion characteristics.

To summarize, the current study demonstrates the feasibility of DBSI to identify coexisting pathologies noninvasively and to potentially serve as a surrogate outcome measure for traumatic SCI at early time-points when behavioral assessments do not correctly reflect the severity of white matter injury.

Acknowledgments

This study was supported in part by the grants from National Institute of Health R01-NS047592 (S.-K.S./W.Z.R), P01-NS059560 (A.H.C.), U01- EY205500 (S.-K.S.), National Multiple Sclerosis Society (NMSS) RG 4549A4/1 (S.-K.S.), FG-1507-05315 (T.-H.L.), Department of Defense Idea Award W81XWH-12-1-0457 (S.-K.S.), and Missouri Spinal Cord Injury Research Program (W.Z.R). AHC was supported in part by the Manny and Rosalyn Rosenthal-Dr. John L. Trotter MS Center Chair in Neuroimmunology of Barnes-Jewish Hospital Foundation.

Author Disclosure Statement

No competing interests exist for all authors.

References

1. Li, Y., Walker, C.L., Zhang, Y.P., Shields, C.B., and Xu, X.M. (2014). Surgical decompression in acute spinal cord injury: a review of clinical evidence, animal model studies, and potential future directions of investigation. Front. Biol. 9, 127–136.
2. Oyinbo, C.A. (2011). Secondary injury mechanisms in traumatic spinal cord injury: a nugget of this multiply cascade. Acta Neurobiol. Exp. 71, 281–299.
3. Bjartmar, C., Wujek, J.R., and Trapp, B.D. (2003). Axonal loss in the pathology of MS: consequences for understanding the progressive phase of the disease. J. Neurol. Sci. 206, 165–171.

4. Criste, G., Trapp, B., and Dutta, R. (2014). Axonal loss in multiple sclerosis: causes and mechanisms. Handb. Clin. Neurol. 122, 101–113.
5. Dutta, R. and Trapp, B.D. (2011). Mechanisms of neuronal dysfunction and degeneration in multiple sclerosis. Prog. Neurobiol. 93, 1–12.
6. Lammertse, D., Dungan, D., Dreisbach, J., Falci, S., Flanders, A., Marino, R., and Schwartz, E. (2007). Neuroimaging in traumatic spinal cord injury: an evidence-based review for clinical practice and research. J. Spinal Cord Med. 30, 205–214.
7. Beaulieu, C. (2002). The basis of anisotropic water diffusion in the nervous system - a technical review. NMR Biomed. 15, 435–455.
8. Song, S.K., Sun, S.W., Ju, W.K., Lin, S.J., Cross, A.H., and Neufeld, A.H. (2003). Diffusion tensor imaging detects and differentiates axon and myelin degeneration in mouse optic nerve after retinal ischemia. NeuroImage 20, 1714–1722.
9. Budde, M.D., Kim, J.H., Liang, H.F., Schmidt, R.E., Russell, J.H., Cross, A.H., and Song, S.K. (2007). Toward accurate diagnosis of white matter pathology using diffusion tensor imaging. Magn. Reson. Med. 57, 688–695.
10. Kim, J.H., Loy, D.N., Liang, H.F., Trinkaus, K., Schmidt, R.E., and Song, S.K. (2007). Noninvasive diffusion tensor imaging of evolving white matter pathology in a mouse model of acute spinal cord injury. Magn. Reson. Med. 58, 253–260.
11. Kim, J.H., Loy, D.N., Wang, Q., Budde, M.D., Schmidt, R.E., Trinkaus, K., and Song, S.K. (2010). Diffusion tensor imaging at 3 hours after traumatic spinal cord injury predicts long-term locomotor recovery. J. Neurotrauma 27, 587–598.
12. Chiang, C.W., Wang, Y., Sun, P., Lin, T.H., Trinkaus, K., Cross, A.H., and Song, S.K. (2014). Quantifying white matter tract diffusion parameters in the presence of increased extra-fiber cellularity and vasogenic edema. Neuroimage 101, 310–319.
13. Tu, T.W., Kim, J.H., Wang, J., and Song, S.K. (2010). Full tensor diffusion imaging is not required to assess the white-matter integrity in mouse contusion spinal cord injury. J. Neurotrauma 27, 253–262.
14. Hausmann, O.N. (2003). Post-traumatic inflammation following spinal cord injury. Spinal cord 41, 369–378.
15. Winklewski, P.J., Sabisz, A., Naumczyk, P., Jodzio, K., Szurowska, E., and Szarmach, A. (2018). Understanding the physiopathology behind axial and radial diffusivity changes—what do we know? Front. Neurol. 9, 92.
16. Grassi, D.C., Conceicao, D.M.D., Leite, C.D.C., and Andrade, C.S. (2018). Current contribution of diffusion tensor imaging in the evaluation of diffuse axonal injury. Arq. Neuropsiquiatr. 76, 189–199.
17. Wang, Y., Wang, Q., Haldar, J.P., Yeh, F.C., Xie, M., Sun, P., Tu, T.W., Trinkaus, K., Klein, R.S., Cross, A.H., and Song, S.K. (2011). Quantification of increased cellularity during inflammatory demyelination. Brain 134, 3590–3601.
18. Wang, X., Cusick, M.F., Wang, Y., Sun, P., Libbey, J.E., Trinkaus, K., Fujinami, R.S., and Song, S.K. (2014). Diffusion basis spectrum imaging detects and distinguishes coexisting subclinical inflammation, demyelination and axonal injury in experimental autoimmune encephalomyelitis mice. NMR Biomed. 27, 843–852.
19. Lin, T.H., Chiang, C.W., Perez-Torres, C.J., Sun, P., Wallendorf, M., Schmidt, R.E., Cross, A.H., and Song, S.K. (2017). Diffusion MRI quantifies early axonal loss in the presence of nerve swelling. J. Neuroinflammation 14, 78.
20. Murphy, R.K.J., Sun, P., Xu, J., Wang, Y., Sullivan, S., Gamble, P., Wagner, J., Wright, N.N., Dorward, I.G., Riew, D., Santiago, P., Kelly, M.P., Trinkaus, K., Ray, W.Z., and Song, S.-K. (2016). Magnetic resonance imaging biomarker of axon loss reflects cervical spondylotic myelopathy severity. Spine (Phila Pa 1976) 41, 751–756.
21. Jakeman, L.B., Guan, Z., Wei, P., Ponnappan, R., Dzwonczyk, R., Popovich, P.G., and Stokes, B.T. (2000). Traumatic spinal cord injury produced by controlled contusion in mouse. J. Neurotrauma 17, 299–319.
22. Kim, J.H., Tu, T.W., Bayly, P.V., and Song, S.K. (2009). Impact speed does not determine severity of spinal cord injury in mice with fixed impact displacement. J. Neurotrauma 26, 1395–1404.
23. Kim, J.H. and Song, S.K. (2013). Diffusion tensor imaging of the mouse brainstem and cervical spinal cord. Nat. Protoc. 8, 409–417.
24. Batchelor, P.G., Atkinson, D., Hill, D.L., Calamante, F., and Connelly, A. (2003). Anisotropic noise propagation in diffusion tensor MRI sampling schemes. Magn. Reson. Med. 49, 1143–1151.
25. Wang, Y., Sun, P., Wang, Q., Trinkaus, K., Schmidt, R.E., Naismith, R.T., Cross, A.H., and Song, S.K. (2015). Differentiation and quantification of inflammation, demyelination and axon injury or loss in multiple sclerosis. Brain 138, 1223–1238.
26. Wang, X., Cusick, M.F., Wang, Y., Sun, P., Libbey, J.E., Trinkaus, K., Fujinami, R.S., and Song, S.K. (2014). Diffusion basis spectrum imaging detects and distinguishes coexisting subclinical inflammation, demyelination and axonal injury in experimental autoimmune encephalomyelitis mice. NMR Biomed. 27, 843–852.
27. Lin, T.H., Kim, J.H., Perez-Torres, C., Chiang, C.W., Trinkaus, K., Cross, A.H., and Song, S.K. (2014). Axonal transport rate decreased at the onset of optic neuritis in EAE mice. Neuroimage 100C, 244–253.
28. Lin, T.H., Spees, W.M., Chiang, C.W., Trinkaus, K., Cross, A.H., and Song, S.K. (2014). Diffusion fMRI detects white-matter dysfunction in mice with acute optic neuritis. Neurobiol. Dis. 67, 1–8.
29. Budde, M.D., Xie, M., Cross, A.H., and Song, S.K. (2009). Axial diffusivity is the primary correlate of axonal injury in the experimental autoimmune encephalomyelitis spinal cord: a quantitative pixelwise analysis. J. Neurosci. 29, 2805–2813.
30. Kim, J.H., Song, S.K., Burke, D.A., and Magnuson, D.S. (2012). Comprehensive locomotor outcomes correlate to hyperacute diffusion tensor measures after spinal cord injury in the adult rat. Exp. Neurol. 235, 188–196.
31. Wang, B., Chen, C., Zhang, J.T., Song, R.X., and Yu, X.C. (2015). Triptolide (TPL) improves locomotor function recovery in rats and reduces inflammation after spinal cord injury. Neurol. Sci. 36, 701–705.
32. Zhang, N., Yin, Y., Xu, S.J., Wu, Y.P., and Chen, W.S. (2012). Inflammation & apoptosis in spinal cord injury. Indian J. Med. Res. 135, 287–296.
33. Assaf, Y., Mayk, A., and Cohen, Y. (2000). Displacement imaging of spinal cord using q-space diffusion-weighted MRI. Magn. Reson. Med. 44, 713–722.
34. Jensen, J.H., Helpern, J.A., Ramani, A., Lu, H., and Kaczynski, K. (2005). Diffusional kurtosis imaging: the quantification of non-gaussian water diffusion by means of magnetic resonance imaging. Magn. Reson. Med. 53, 1432–1440.
35. Raz, E., Bester, M., Sigmund, E.E., Tabesh, A., Babb, J.S., Jaggi, H., Helpern, J., Mitnick, R.J., and Inglese, M. (2013). A better characterization of spinal cord damage in multiple sclerosis: a diffusional kurtosis imaging study. AJNR Am. J. Neuroradiol. 34, 1846–1852.
36. Assaf, Y. and Basser, P.J. (2005). Composite hindered and restricted model of diffusion (CHARMED) MR imaging of the human brain. NeuroImage 27, 48–58.
37. Assaf, Y., Freidlin, R.Z., Rohde, G.K., and Basser, P.J. (2004). New modeling and experimental framework to characterize hindered and restricted water diffusion in brain white matter. Magn. Reson. Med. 52, 965–978.
38. Zhang, H., Schneider, T., Wheeler-Kingshott, C.A., and Alexander, D.C. (2012). NODDI: practical in vivo neurite orientation dispersion and density imaging of the human brain. NeuroImage 61, 1000–1016.
39. By, S., Xu, J., Box, B.A., Bagnato, F.R., and Smith, S.A. (2017). Application and evaluation of NODDI in the cervical spinal cord of multiple sclerosis patients. NeuroImage. Clinical 15, 333–342.
40. Byrnes, K.R., Fricke, S.T., and Faden, A.I. (2010). Neuropathological differences between rats and mice after spinal cord injury. J. Magn. Reson. Imaging 32, 836–846.
41. Van Asseldonk, J.T.H., Van den Berg, L.H., Kalmijn, S., Van den Berg-Vos, R.M., Polman, C.H., Wokke, J.H.J., and Franssen, H. (2006). Axon loss is an important determinant of weakness in multifocal motor neuropathy. J. Neurol. Neurosurg. Psychiatry 77, 743–747.
42. DeLuca, G.C., Ebers, G.C., and Esiri, M.M. (2004). Axonal loss in multiple sclerosis: a pathological survey of the corticospinal and sensory tracts. Brain 127, 1009–1018.
43. Medana, I.M. and Esiri, M.M. (2003). Axonal damage: a key predictor of outcome in human CNS diseases. Brain 126, 515–530.
44. Dumont, R.J., Okonkwo, D.O., Verma, S., Hurlbert, R.J., Boulos, P.T., Ellegala, D.B., and Dumont, A.S. (2001). Acute spinal cord injury, part I: pathophysiologic mechanisms. Clin. Neuropharmacol. 24, 254–264.

Address correspondence to:
Sheng-Kwei Song, PhD
Washington University School of Medicine
Biomedical MR Laboratory
Campus Box 8227
4525 Scott Avenue, Room 2313
St. Louis, MO 63110

E-mail: ssong@wustl.edu